O.N. Forde, K.U. Mayer, and A.G. Cahill, Dep. of Earth, Ocean and Atmospheric Sciences, Univ. of British Columbia, 2007 Main Mall, Vancouver, BC, V6T 1Z4, Canada; B. Mayer, Dep. of Geoscience, Univ. of Calgary, 2500 University Drive NW, Calgary, AB, T2N 1N4, Canada; A.G. Cahill, J.A. Cherry, and B.L. Parker, G360 Institute for Groundwater Research, College of Engineering & Physical Sciences, Univ. of Guelph, 50 Stone Road East, Guelph, ON, N1G 2W1, Canada. *Corresponding author (oforde@eos.ubc.ca).

Vadose Zone Gas Migration and Surface Effluxes after a Controlled Natural Gas Release into an Unconfined Shallow Aquifer

O.N. Forde,* K.U. Mayer, A.G. Cahill, B. Mayer, J.A. Cherry, and B.L. Parker

Shale gas development has led to concerns regarding fugitive CH_4 migration in the subsurface and emissions to the atmosphere. However, few studies have characterized CH_4 migration mechanisms and fate related to fugitive gas releases from oil or gas wells. This paper presents results from vadose zone gas and surface efflux monitoring during a natural gas release experiment at Canadian Forces Base Borden, Alliston, Ontario, Canada. Over 72 d, 51 m^3 of natural gas (>93% CH_4) was injected into a shallow, unconfined sand aquifer at depths of 4.5 and 9 m. Methane and CO_2 effluxes in combination with soil gas concentrations and stable C isotopic signatures were used to quantify the spatiotemporal migration and fate of injected gas. Preferential gas migration pathways led to vadose zone hot spots, with CH_4 concentrations exceeding the lower explosive limit (5% v/v). From these hot spots, episodic surface CH_4 effluxes (temporally exceeding 2500 μmol m^{-2} s^{-1} [3465 g m^{-2} d^{-1}]) occurred during active injection. Higher injection rates led to increased average CH_4 effluxes and greater lateral migration, as evidenced by a growing emission area approaching 25 m^2 for the highest injection rate. Reactive transport modeling showed that high CH_4 fluxes resulted in advection-dominated migration and limited CH_4 oxidation, whereas lower CH_4 effluxes were diffusion dominated with substantial CH_4 oxidation. These results and our interpretations allowed us to develop a conceptual model of fugitive CH_4 migration from the vadose zone to the ground surface.

Abbreviations: CFB, Canadian Forces Base; GM, gas migration; RTM, reactive transport model; VWC, volumetric water content.

The rise in shale gas development has heightened concerns on the potential impacts of fugitive CH_4 emissions to the subsurface and atmosphere (Jackson et al., 2014). Methane (the primary component of natural gas) is a greenhouse gas of concern due to its global warming potential that is 86 times greater than that of CO_2 over 20 yr and 25 times greater over 100 yr (Myhre et al., 2013). Methane can be released to the atmosphere through surface casing vent flows and/or to the subsurface and atmosphere from stray gas migration (GM). Both pathways are a result of imperfectly sealed oil and gas wells. In the case of GM, gas enters the subsurface along a leaky well bore and, driven by its buoyancy, migrates upward toward overlying freshwater aquifers and the vadose zone (Davies et al., 2014; Dusseault and Jackson, 2014). Methane migration as a result of well integrity failure is well documented in the oil and gas industry and, aside from surface casing vent flows, continues to pose the most likely pathway for gas to reach the ground surface (Davies et al., 2014; Dusseault and Jackson, 2014; Dusseault et al., 2000; Erno and Schmitz, 1996; Hammond, 2015; Harrison, 1983, 1985; Watson and Bachu, 2009). In Alberta, Canada, a recent report estimated that 0.73% of 3276 wells had compromised well casings resulting in GM (Bachu, 2017). In the United Kingdom, elevated CH_4 soil gas concentrations at 30% of 102 abandoned and decommissioned oil and gas wells were attributed to GM (Boothroyd et al., 2016). Various studies have also reported the occurrence of GM from faulty well casings via the detection of dissolved CH_4 in aquifers (Darrah et al., 2014; Jackson et al., 2013; Osborn et al., 2011) and CH_4 emissions to the atmosphere (Allen et al., 2013; Caulton et al., 2014; Johnson et al., 2017; Kang et al., 2016; Lan et al., 2015).

Although these studies have traced the origin of fugitive CH_4 to leakage from compromised well casings, there is a need to better understand the pathways and mechanisms of fugitive CH_4 migration at a scale that is appropriate to a single extraction well and for a leakage event of known magnitude and duration (Council of Canadian Academies, 2014).

Research on gas transport mechanisms in porous media (including CH_4 GM) has shown that small-scale heterogeneities may result in lateral and discontinuous gas transport (Gorody, 2012; Mumford et al., 2010; Steelman et al., 2017; Tomlinson et al., 2003). Methane release from the saturated zone into the vadose zone may occur if buoyancy forces are great enough to overcome capillary forces (Gorody, 2012). In addition, gas release to the vadose zone may be influenced by barometric pressure and water table fluctuations (Baird et al., 2004; Strack and Waddington, 2008; Strack et al., 2006; Zhang et al., 2012). Vertical GM can result in surface effluxes of CH_4 and CO_2, as previously shown at petroleum hydrocarbon spill sites (Sihota et al., 2013). In the presence of oxygen (O_2), CH_4 can undergo aerobic oxidation driven by methanotrophs to produce CO_2 (Bogner et al., 1997). Significant CH_4 and CO_2 effluxes due to GM from imperfectly sealed oil and gas wells pose a global environmental concern for greenhouse gas emissions and a local risk of explosion if CH_4 concentrations in soil gas exceed 5% (v/v). Various studies have used numerical modeling to characterize the fate and transport of CH_4 gas due to well bore leakage in the saturated zone (Nowamooz et al., 2015; Rice et al., 2018; Roy et al., 2016). However, in the context of fugitive GM, no studies to our knowledge have conducted numerical modeling of the transport and reaction mechanisms affecting the fate of CH_4 in the vadose zone. Numerical models suitable for simulation of the fate of CH_4 in the vadose zone are available. For example, Sihota and Mayer (2012) and Molins et al. (2008) used reactive transport modeling (RTM) to characterize gas transport and reaction processes at a site contaminated with petroleum hydrocarbons and in landfill covers, respectively. Without a comprehensive understanding of the migration and fate of fugitive CH_4, it remains difficult to delineate and quantify emissions to the atmosphere related to GM originating from oil and gas wells.

Recently, a controlled subsurface natural gas release experiment was conducted at the Canadian Forces Base (CFB) Borden, Alliston, Ontario, Canada. Over 72 d, 51 m^3 of natural gas (>93% CH_4) was injected at depths of 4.5 and 9 m in a shallow, unconfined sand aquifer (Cahill et al., 2017, 2018; Steelman et al., 2017). Below the water table, free-phase CH_4 migration was influenced by small-scale heterogeneities and resulted in extensive lateral GM downgradient of the injection location (Cahill et al., 2018). Episodic releases of free-phase gas were measured at the ground surface as CH_4 effluxes. Measurements over 12 d of the 72-d experiment demonstrated both spatial and temporal variability of gas effluxes, despite the proximity of measurement locations to the injection point and a continuous injection rate (Cahill et al., 2017). Cahill et al. (2017) also suggested that a substantial portion of the injected CH_4 was lost to oxidation in the vadose zone, whereas minimal oxidation occurred in the saturated zone during the period of gas injection. Although Cahill et al. (2017) provided an overview of the study results, including vadose zone responses, a detailed analysis of CH_4 GM mechanisms and fate from the vadose zone to the ground surface for the entire duration of the experiment was not provided.

The current contribution focuses on the interpretation of the complete data set, including spatial and temporal effluxes for CH_4 and CO_2, vadose zone soil gas concentrations, and stable carbon isotope ratios measured over the 89-d experiment encompassing baseline monitoring, all injection phases, and the recovery period after injection. Results are supplemented with quantitative and process-based RTM to identify the dominant transport and reaction mechanisms affecting CH_4 for a range of CH_4 effluxes. The overall goal of this study is to contribute to a better understanding of the spatial distribution, temporal evolution, migration, and fate of CH_4 in the vadose zone and the potential for fugitive gas emissions to the atmosphere.

Specific objectives of this study were (i) to evaluate the magnitude and spatiotemporal distribution of surficial CH_4 and CO_2 effluxes as a function of gas injection rates, (ii) to assess the evolution of GM processes and CH_4 oxidation in the vadose zone, (iii) to estimate the fraction of injected CH_4 lost from the saturated zone and emitted to the atmosphere as CH_4, and (iv) to discuss the implications for monitoring and detecting fugitive CH_4.

Materials and Methods
Site Description and Natural Gas Injection

A controlled natural gas release experiment was conducted at the CFB Borden, Alliston, Ontario, Canada. The shallow, unconfined glacio-lacustrine sand aquifer at the site has been well characterized through various studies (Sudicky and Illman, 2011), allowing for a focused analysis on the fate and transport of fugitive CH_4. The aquifer extends 7 to 9 m below the ground surface and is underlain by a silt aquitard. The aquifer contains horizontal discontinuous lenses of medium-grained, fine-grained, and silty fine-grained sand with infrequent silt, silty-clay, and coarse sand layers (Sudicky and Illman, 2011). The water table is located 1 m ($\pm$0.5 m) below the ground surface, providing an opportunity to study GM representative for sites with a shallow water table. Such conditions occur, for example, at some oil and gas plays in northeastern British Columbia, Canada (Ferbey et al., 2008).

Over 72 d, 51 m^3 (at 0.1013 MPa and 15°C) of natural gas (93.8% CH_4, 3.8% C_2H_6, 0.3% C_3H_8, ∼0.1% C_{4+}, 1.1% N_2, 0.8% CO_2, 0.05% O_2) was injected using inclined sparging wells at depths of 4.5 and 9 m below ground surface (Fig. 1). The injection wells were installed at a 45° angle to minimize vertical CH_4 migration along the well. Wells were installed using a Geoprobe (model 7822DT) direct push system in a vertical plane perpendicular to groundwater flow. Natural gas was injected from gas canisters
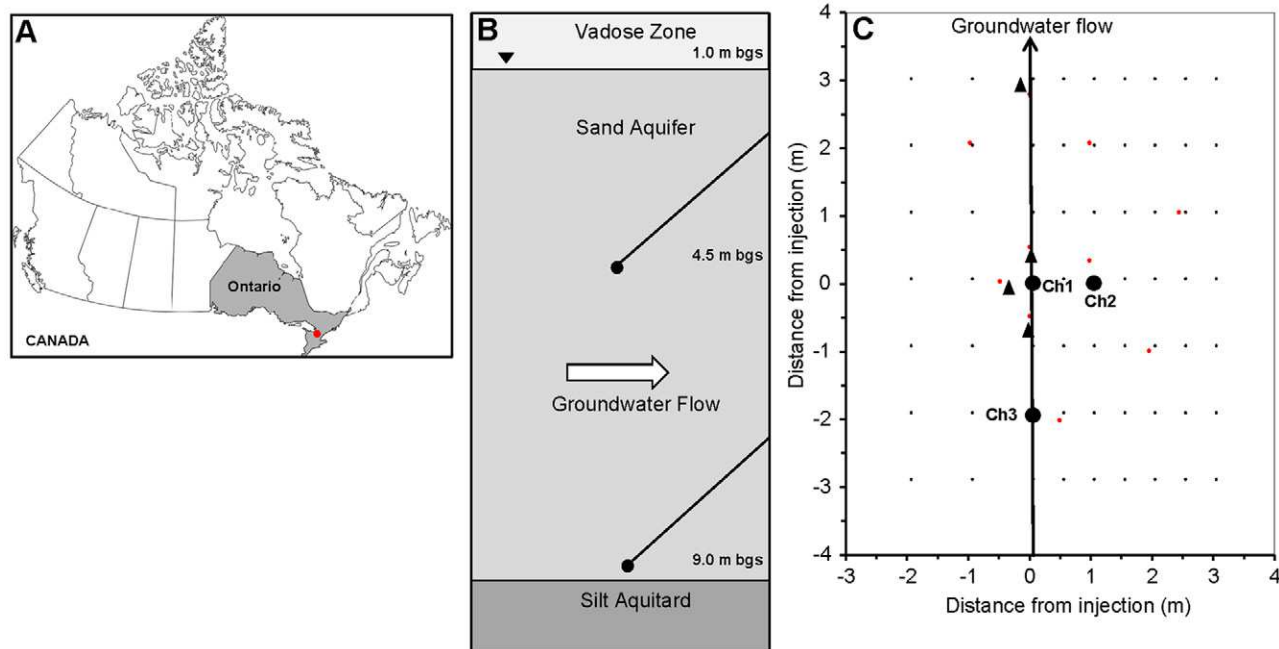
Fig. 1. (A) Map of Canada with the location of the Canadian Forces Base Borden in Ontario marked by a red dot. (B) Borden aquifer hydrological setting with a thin vadose zone and a relatively homogenous sand aquifer underlain by a silt aquitard. Injection points are labeled at their respective depths below ground surface (bgs). (C) Monitoring network. Small black dots represent survey efflux measurement locations; large black dots indicate long-term chambers Ch1, Ch2, and Ch3 as labeled; triangles indicate sensor locations; red dots represent soil gas monitoring wells at depths of 10, 30, and 50 cm.

connected via polyethylene tubing to the injection ports. Injection rates were adjusted incrementally and controlled by in-line electronic mass flow controllers (Red-y smart GSC-C9SA-BB26) with the associated software (Get Red-y, Vögtlin Instruments AG). When the injection phases were completed (Day 72), the wells were sealed with no-return valves to prevent flow-back of gas.

The varying injection rates of the experiment are categorized into five phases, including the recovery period after injection (Table 1). The injection rate increased from Phase 1 to Phase 4; however, the shallow injection well (4.5 m) was turned off in Phase 3. Surface casing vent flows indicate leakage within a well and can be used as a proxy for the occurrence of GM. Gas injection rates were based on reported surface casing vent flows from Alberta and British Columbia, Canada (Nowamooz et al., 2015), assuming that leaky wells could lead to GM of similar magnitude. Vadose zone and surficial monitoring commenced 2 d prior to and continued until 15 d after the end of injection, corresponding to a period of investigation of 89 d.

Soil Gas Effluxes

Three long-term dynamic closed chambers (LI-8100-104, LI-COR Inc.) were used in combination with a multiplexer (LI-8150, LI-COR Inc.) and a CO_2 infra-red gas analyzer (LI-8100, LI-COR Inc.) to monitor water vapor and CO_2 effluxes throughout the experiment (Fig. 1). Coupled with these instruments, water vapor, CH_4, and CO_2 effluxes were measured with an extended-range (0.01–100,000 ppm) ultraportable greenhouse gas analyzer (Los Gatos Research Inc.). Measurements were conducted approximately

every 15 min at each chamber. Periodically, the long-term chambers were disconnected to complete survey measurements (over ∼2 to 6 h) on a monitoring grid including up to 63 locations (Fig. 1). Measurements were completed with a survey chamber (LI-8100-103, LI-COR Inc.) connected to the infrared gas analyzer and the ultraportable greenhouse gas analyzer. The instrumental setup for the flux measurements followed the approach by Sihota et al. (2013).

The survey and long-term chambers were placed on preinstalled polyvinyl chloride collars (20 cm i.d.) covering an area of 317.8 cm^2. The collars were inserted at least 4 cm into the soil 1 wk prior to commencing the gas injection to allow soil gas effluxes to equilibrate (Law et al., 2001). Long-term chambers were colocated with in-soil volumetric water content (VWC), electrical conductivity, temperature sensors, and soil gas sampling ports. The purpose of the long-term chambers was to monitor the temporal evolution of effluxes at selected locations close to the injection well. The survey measurements were completed to periodically monitor the spatial distribution of effluxes

Table 1. Experimental phases for natural gas injection and recovery periods.

Phase	Duration	Shallow injection rate	Deep injection rate	Total rate
	d	——— L min^{-1} ———		L d^{-1}
I	28	0.06	0.06	172.8
II	40	0.35	0.35	1008
III	2	0	0.35	504
IV	2	1.5	1.5	4320
V	15	0	0	0

(Fig. 1). In addition, effluxes at one background location (outside the monitoring area shown in Fig. 1 but with similar vegetation) were measured with every survey campaign.

Soil gas effluxes (F, in μmol m^{-2} s^{-1} or g m^{-2} d^{-1}) were calculated using well-established methods based on measured concentration changes in the chamber over the specified time interval ($\partial C/\partial t$) and the measured water vapor content (W), pressure (P), temperature (T), system volume (V), and measurement area (S) (LI-COR, 2015):

$$F = \frac{10VP\left(1-W/1000\right)}{RS\left(T+273.15\right)} \frac{\partial C}{\partial t} \qquad [1]$$

where F is the soil gas efflux rate (μmol m^{-2} s^{-1}); P is the initial pressure (kPa); T is the initial air temperature ($^{\circ}$C); W is the initial water vapor model fraction (mmol mol^{-1}); V is the total system volume including chamber, analyzers, tubing, and soil collar (cm^3); R is the ideal gas constant (8.314 Pa m^3 K^{-1} mol^{-1}); S is the soil surface area underneath the soil collar (cm^2); and $\partial C/\partial t$ is the initial rate of change of the water-corrected CO_2 or CH_4 mole fraction during measurement period (μmol mol^{-1} s^{-1}).

The chamber measurements were conducted for a period of 2.5 min. Observed linear concentration increases with durations ranging from 45 to 80 s were used to calculate the effluxes. Previous work has demonstrated that a linear approximation can be used effectively to compute effluxes for measurement durations in this range (Alm et al., 2007; Heijmans et al., 2004). Compared with an exponential regression, a linear approximation tends to provide a more conservative estimate of the efflux and thus reduces the risk of overestimation (Forbrich et al., 2010; Pihlatie et al., 2013). Average, minimum, and maximum CH_4 and CO_2 effluxes were calculated for each injection phase, excluding the 5-d power outage on Day 39 when no data were collected.

Soil Gas Sampling

Soil gas samples were collected from monitoring wells that were installed at 10 selected locations at depths of 10, 30, and 50 cm (Fig. 1). The monitoring wells consisted of 1/8-in gas impermeable polyethylene tubing with a mesh screen attached to the bottom and a gas-tight fitting and septa at the top. Three line volumes were purged using gas-tight syringes (Valco Instruments Co.). Samples were collected and stored in pre-evacuated 12-mL vials (Labco Ltd.). Gas composition analyses (CH_4, CO_2, N_2, O_2, and Ar) were completed at the University of British Columbia on a Varian MicroGC CP-4900 dual-channel gas chromatograph equipped with a MolSieve 5a column (for O_2, N_2 and Ar), a PoraPlot Q column (for CH_4 and CO_2), and micro-machined thermal conductivity detectors. The method of analysis on the GC followed Amos et al. (2005) and Sihota et al. (2011). Stable carbon isotope ratios ($^{13}C/^{12}C$) of CH_4 and CO_2 were measured in the Isotope Science Laboratory at the University of Calgary (Alberta, Canada). Analyses were completed on a ThermoFisher MAT 253 isotope ratio mass spectrometer coupled to Trace GC Ultra + GC Isolink (ThermoFisher) (Humez et al., 2016). Results are reported in the internationally accepted delta (δ^{13}C) notation (in ‰) relative to Vienna PeeDee Belemnite (VPDB) with a precision better than ±0.5 and ±0.3‰ for δ^{13}C values of CH_4 and CO_2, respectively.

Volumetric Water Content and Barometric Pressure

A datalogger (CR-1000, Campbell Scientific) was used to collect data from in-soil sensors for VWC, electrical conductivity, and temperature (CS650, Campbell Scientific). Sensors were placed 50 cm below the ground surface at four selected locations next to gas sampling ports and long-term chambers (Fig. 1). Barometric pressure was continuously recorded with a pressure transducer installed at the field site (Baro-Diver, vanEssen Instruments).

Mass Balance Calculations

Mass balance calculations were conducted using long-term and survey efflux data to estimate daily and cumulative CH_4 mass losses to the atmosphere. A detailed description of the methodology of the mass balance calculation can be found in the Supplemental Material.

Reactive Transport Modeling

The MIN3P-DUSTY RTM (Molins and Mayer, 2007) was used to quantitatively assess the subsurface fate of CH_4. MIN3P-DUSTY accounts for geochemical reactions in the vadose zone, multicomponent solute transport, and advective-diffusive multicomponent gas transport. Gas diffusion is described by the Dusty Gas Model (Mason and Malinauskas, 1983; Sihota and Mayer, 2012) with species-dependent binary diffusion coefficients. Gas phase tortuosity is described with the Millington (1959) formulation (Sihota and Mayer, 2012). MIN3P-DUSTY has previously been used to simulate transport and reactions processes involving CH_4 at a hydrocarbon-contaminated site (Molins et al., 2010; Sihota and Mayer, 2012) and in landfill cover soils (Molins et al., 2008), confirming that the code is well suited for the process-based assessment of vadose zone CH_4 fate and transport in the current experiment.

Two simulations were completed targeting high and low CH_4 efflux conditions constrained by observations at Chamber 2 and the associated multilevel soil gas sampling well. Each simulation was completed using a one-dimensional domain describing a 70-cm soil column to represent the vertical extent of the vadose zone at the CFB Borden field site. The physical properties of the soil were selected based on literature values from previous experiments conducted at the site (Table 2). Gas concentrations at the upper boundary were fixed at atmospheric levels. Binary free-phase gas diffusion coefficients and viscosities were adopted from Sihota and Mayer (2012).

Reactive GM through the vadose zone was simulated for the low- and high-flow-rate regimes by applying a specified CH_4 influx at the base of the soil column, corresponding to the

observed total gas efflux ($CO_2 + CH_4$) for the relevant flow rate regime. The total influx introduced for the low-flux simulation was 6.7 µmol m^{-2} s^{-1} (9.3 g CH_4 m^{-2} d^{-1}) and 113.9 µmol m^{-2} s^{-1} (157.8 g CH_4 m^{-2} d^{-1}) for the high-flux regime. The gas introduced was assumed to have the same carbon isotope ratio as the injected CH_4 (δ^{13}C-CH_4 −42‰). The δ^{13}C values for CO_2 in the injected gas (−10‰) and produced by root respiration (−22‰) were defined to represent values found in thermogenic shale gas (Dai et al., 2017; Golding et al., 2013) and in the organic horizon of soils (e.g., Bird and Pousai, 1997), respectively. The aerobic oxidation of CH_4, including carbon isotope fractionation, was simulated following the approach of Sihota and Mayer (2012) (Table 3). A kinetic fractionation model was used to account for the preferred oxidation of ^{12}C-CH_4 leading to the enrichment of ^{12}C-CO_2 in soil gas (Sihota and Mayer, 2012). Reaction rates for CH_4 oxidation for high- and low-flux events were calibrated to reproduce field observations (Table 3). Following Sihota and Mayer (2012), it was assumed that close to 50% of the carbon oxidized during the CH_4 degradation process was sequestered in biomass (Table 3). Root respiration with its own characteristic carbon isotope signature (−22‰) was also considered to contribute to CO_2 production in the upper 20 cm of the vadose zone. Calibrated reaction rates for root respiration were similar to those reported by Sihota and Mayer (2012) and Trumbore (2000) (Table 3).

The model was constrained by using data from high- and low-flux events from one vertical well, including data on VWCs, soil gas concentrations (CH_4, CO_2, N_2, and O_2), stable carbon isotope ratios of CH_4 and CO_2, and CH_4 and CO_2 effluxes. Due to the limited availability of vadose zone molecular and isotopic gas data, simulations were completed to represent steady-state conditions for the respective flow rate regimes. Recharge was set at 300 mm yr^{-1} to obtain water contents ranging from 0.27 near the base of the domain to 0.15 near the surface, consistent with field observations.

Table 2. Soil parameters used for low and high flux model simulations.

Parameter	Value	Reference
Hydraulic conductivity, m s^{-1}	6.5×10^{-5}	Allen-King et al. (1998)
van Genuchten parameters		
α, m^{-1}	2.0	Sudicky et al. (2010)
n	1.9	
Residual saturation, m^3 H_2O m^{-3} porous medium	0.06	Sudicky et al. (2010)
Porosity, m^3 void m^{-3} porous medium	0.35	Sudicky et al. (2010)

Results and Discussion

Magnitude and Spatiotemporal Distribution of Effluxes as a Function of Gas Injection Rates

Baseline CH_4 effluxes were monitored for 2 d prior to initiating the gas injection and remained nondetectable during this time. Within 5 h of commencing the injection (0.04 m^3 CH_4 injected), CH_4 effluxes were observed at the surface. Throughout Phase 1, average CH_4 effluxes remained relatively constant, with values of 2.4, 8.8, and 0.01 µmol m^{-2} s^{-1} (3.3, 12.2, and 0.01 g CH_4 m^{-2} d^{-1}) for Chambers 1, 2, and 3, respectively (Table 4; Fig. 2). As the injection rate increased in Phase 2, effluxes increased, with average CH_4 effluxes at Chambers 1, 2, and 3 reaching 10.1, 64.3, and 3.3 µmol m^{-2} s^{-1} (14.0, 89.1, and 4.6 g CH_4 m^{-2} d^{-1}), respectively. Effluxes continued to rise in response to the highest injection rate in Phase 4, reaching 33.9, 98.5, and 5.5 µmol m^{-2} s^{-1} (46.9, 136.5, and 7.6 g CH_4 m^{-2} d^{-1}) at Chambers 1, 2, and 3, respectively, within 4 h (Tables 1 and 4). Methane effluxes showed an equally rapid response when the injection system was turned off. In Phase 3, when the 4.5-m injection well was turned off, CH_4 effluxes declined drastically to 3.6, 11.0, and 1.1 µmol m^{-2} s^{-1} (5.0, 15.2, and 1.5 g CH_4 m^{-2} d^{-1}) at Chambers 1, 2, and 3, respectively, within 6 h (Table 4; Fig. 2). In Phase 5, when the experimental

Table 3. Reaction stoichiometry and rate constants for low and high CH_4 flux simulations.

Process	Stoichiometry rate expression (R)	Rate, Monod, and inhibition constants†
	Low CH_4 flux simulation	
Root respiration	$CH_2O + O_2 \rightarrow CO_2 + H_2O$	$k_{CH2O} = 1.7 \times 10^{-8}$ mol dm^{-3} s^{-1}
Methane oxidation	$CH_4 + 1.515O_2 \rightarrow 0.515CO_2 + 1.1515H_2O + 0.485CH_2O(\text{biomass})$ $R = -k_{CH4}[C_{CH4}/(K^S_{CH4} + C_{CH4})][C_{O2}/(K^S_{O2} + C_{O2})]$	$k_{CH4} = 1.5 \times 10^{-8}$ mol L^{-1} H_2O s^{-1}
		$K^S_{12CH4} = 1.0 \times 10^{-5}$ mol L^{-1} H_2O
		$K^S_{13CH4} = 8.1 \times 10^{-8}$ mol L^{-1} H_2O
		$K^S_{O2} = 3.1 \times 10^{-6}$ mol L^{-1} H_2O
	High CH_4 flux simulation	
Root respiration	$CH_2O + O_2 \rightarrow CO_2 + H_2O$	$k_{CH2O} = 2.0 \times 10^{-8}$ mol dm^{-3} s^{-1}
Methane oxidation	$CH_4 + 1.515O_2 \rightarrow 0.515CO_2 + 1.1515H_2O + 0.485CH_2O(\text{biomass})$ $R = -k_{CH4}[C_{CH4}/(K^S_{CH4} + C_{CH4})][C_{O2}/(K^S_{O2} + C_{O2})]$	$k_{CH4} = 8.5 \times 10^{-8}$ mol L^{-1} H_2O s^{-1}
		$K^S_{12CH4} = 1.0 \times 10^{-5}$ mol L^{-1} H_2O
		$K^S_{13CH4} = 8.1 \times 10^{-8}$ mol L^{-1} H_2O
		$K^S_{O2} = 3.1 \times 10^{-6}$ mol L^{-1} H_2O

† K^S_i, half-saturation constant for the ith species; k_i, rate constant for the ith species.

Table 4. Soil gas effluxes throughout the experiment from all three chambers. Averages were determined using all long-term efflux measurements excluding the time period of the power outage.

Chamber	Statistic	Soil gas efflux			
		Phase 1	Phase 2	Phase 3	Phase 4
		——————— μmol m^{-2} s^{-1} ———————			
		CH$_4$ efflux			
1	avg.	2.38	10.12	3.62	33.89
	min.	ND	0.02	ND	0.01
	max.	15.84	32.91	22.37	79.05
	SD	1.54	5.39	7.59	20.61
2	avg.	8.76	64.26	11.04	98.52
	min.	ND†	1.18	ND	ND
	max.	122.50	2679	78.20	394.8
	SD	15.19	178.94	25.83	123.40
3	avg.	0.01	3.26	1.12	5.54
	min.	ND	ND	0.64	0.03
	max.	0.36	10.16	3.20	19.14
	SD	0.05	1.68	0.65	7.94
		CO$_2$ efflux			
1	avg.	7.49	18.05	14.43	21.16
	min.	1.13	1.30	1.02	8.02
	max.	28.92	52.67	25.09	40.05
	SD	1.54	5.39	7.59	20.61
2	avg.	11.19	42.69	28.02	31.18
	min.	1.15	2.49	1.09	4.10
	max.	46.11	1006	47.41	74.47
	SD	6.43	56.25	7.68	16.40
3	avg.	6.86	11.71	5.38	9.16
	min.	1.60	1.71	1.13	4.57
	max.	37.09	31.49	15.50	14.67
	SD	2.56	5.06	3.19	1.87

† Nondetectable.

injection was complete by Day 72, CH$_4$ effluxes dissipated to nondetectable within 14 h at Chamber 1, 26 h at Chamber 2, and 45 h at Chamber 3. These results demonstrate that CH$_4$ release rates at the ground surface dynamically and rapidly respond to changes in subsurface injection rates and that surface release rates are a function of injection depth, as evidenced by the rapid decline of surface emissions during Phase 3.

However, effluxes did not reach steady-state conditions during each phase but fluctuated by typically two orders of magnitude at individual measurement locations despite constant injection rates (Fig. 2; Table 4). Although the highest injection rate was applied during Phase 4, the maximum CH$_4$ efflux at Chamber 2 was measured in Phase 2 (2679 μmol m^{-2} s^{-1} [3713 g CH$_4$ m^{-2} d^{-1}]) (Table 4; Fig. 2). During these episodic efflux events, CH$_4$ effluxes rapidly increased and then decreased over a few hours. For example, on Day 26 of Phase 1, CH$_4$ effluxes at

Chamber 2 increased from 4.0 to 120.1 μmol m^{-2} s^{-1} (5.5–166.4 g CH$_4$ m^{-2} d^{-1}) over 9 h and then decreased back to 4.0 μmol m^{-2} s^{-1} (5.5 g CH$_4$ m^{-2} d^{-1}) over 16 h. Peak effluxes at Chambers 1 and 3 were often not temporally correlated with the highest emissions measured at Chamber 2 (Fig. 2).

These episodic emission events can likely be explained by the periodic release of stored gas from the saturated zone. The observed behavior is consistent with free gas accumulation in the saturated zone in response to the injection, which led to pressure build-up that allowed the entrapped gas to overcome capillary forces and develop continuous pathways toward the vadose zone. The low solubility of CH$_4$ gas (31 mg L^{-1} at 298.15 K and 100 kPa) contributed to the accumulation of free-phase gas in the subsurface during active gas injection. Geophysical and dissolved gas data (Cahill et al., 2017, 2018; Steelman et al., 2017) provide additional evidence for the buildup of free-phase gas below the water table. When gas inflow ceased (Phase 3 and Phase 5), total gas pressure in the subsurface dissipated and thus effluxes to the surface rapidly declined (Fig. 2).

Periodic surficial gas releases have also been reported for in situ air sparging studies (Johnson et al., 1993; Selker et al., 2006). During in situ air sparging, pressure buildup from continuous inflow of compressed air allows the gas to overcome capillary forces and displace pore water. As sparging continues, injected gas migrates along the path of least resistance (McCray and Falta, 1996), ultimately finding a pathway through or around low-permeability layers until breakthrough at surface. Upon loss of injection pressure, surface effluxes tend to decline rapidly (Selker et al., 2006; Tomlinson et al., 2003). These observations are consistent with the CH$_4$ migration patterns seen in the present study.

Thus, the observed localized episodic CH$_4$ effluxes are indicative of hydrostratigraphic traps leading to accumulations and intermittent releases of over-pressurized gas. However, despite significant fluctuations within each of the phases (Fig. 2), the magnitude of average CH$_4$ emission rates correlated well with increasing injection rates (Table 4).

Generally, CO$_2$ effluxes also displayed strong temporal variations and increased from Phase 1 to Phase 2 (Fig. 2). Average background CO$_2$ effluxes ranged from 0.7 to 3.0 μmol m^{-2} s^{-1} (2.7–11.4 g CO$_2$ m^{-2} d^{-1}) across all three long-term chambers. Effluxes increased during Phase 1 to averages of 7.5, 11.1, and 6.9 μmol m^{-2} s^{-1} (28.5, 42.2, and 26.2 g CO$_2$ m^{-2} d^{-1}) at Chambers 1, 2, and 3, respectively. Effluxes continued to rise in Phase 2, with averages of 18.1, 42.7, and 11.7 μmol m^{-2} s^{-1} (68.8, 162.4, and 44.5 g CO$_2$ m^{-2} d^{-1}) at Chambers 1, 2, and 3, respectively (Table 4). Although the injected gas contained some CO$_2$, the strong temporal increase of CO$_2$ effluxes provides clear evidence for the occurrence of microbially mediated CH$_4$ oxidation. This observation is in stark contrast to what was observed in the saturated zone, where the isotopic signature of the injected CH$_4$ remained similar to the injected gas for >100 d after injection, suggesting limited CH$_4$ oxidation below the water table (Cahill et al., 2018). Effluxes declined in Phase 3, when the shallow injection
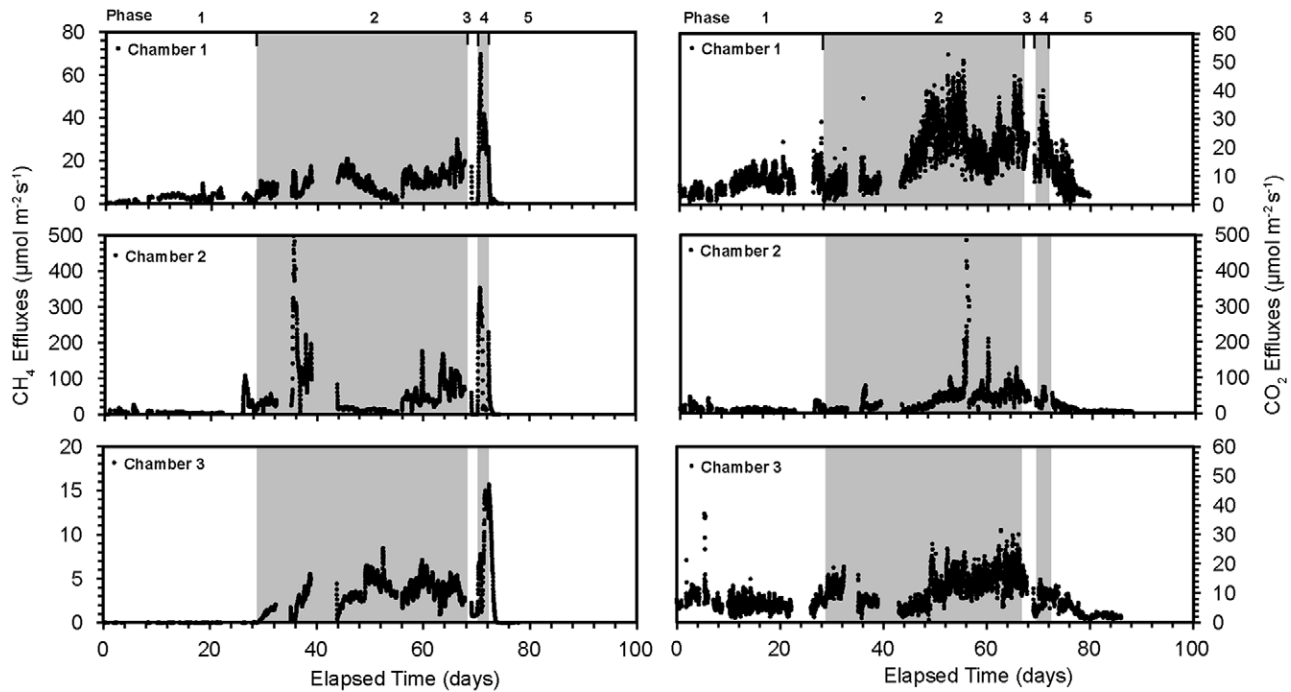
Fig. 2. Effluxes of CH_4 and CO_2 for long-term Chambers 1, 2, and 3 during injection Phases 1 to 4 and recovery Phase 5. Methane effluxes respond rapidly to changes in injection rates and are positively correlated; CO_2 effluxes generally also increase in response to the gas injection. Both CH_4 and CO_2 effluxes are characterized by strong temporal fluctuations independent of the injection rates.

well was turned off, but not as drastically as CH_4 effluxes; average CO_2 effluxes were 14.4, 28.0, and 5.4 μmol m^{-2} s^{-1} (54.8, 106.5, and 20.5 g CO_2 m^{-2} d^{-1}) for Chambers 1, 2, and 3, respectively (Table 4; Fig. 2). The limited decline of CO_2 effluxes during Phase 3 suggests that CH_4 degradation was still occurring and that CH_4 was still released into the vadose zone, although at lower rates. During Phase 4, which had the highest injection rate, average CO_2 effluxes did not differ largely compared with those measured in Phase 2 and were only higher at Chamber 1 (by a factor of 1.2) (Table 4; Fig. 2). At Chambers 2 and 3, average CO_2 effluxes decreased in comparison to Phase 2, reaching only 70 to 80% of observed average Phase 2 effluxes (Table 4). The fact that CO_2 effluxes did not increase further or even declined during the highest injection rate suggests that CH_4 oxidation was inhibited by O_2 displacement from the vadose zone, which can be caused by substantial advective CH_4 effluxes (Molins et al., 2008). The longer persistence in CO_2 effluxes compared with CH_4 effluxes in Phase 5 suggests that residual CH_4 present in the vadose zone, or released from the saturated zone, continued to undergo oxidation (Fig. 2).

Results from survey measurements provide additional insight and demonstrate how the phased gas injection influenced the spatial distribution and magnitude of CH_4 and CO_2 effluxes. Results indicate greater lateral migration across the site in response to increasing injection rates. Throughout the experiment, CH_4 effluxes were relatively contained within a continuous hot spot in close proximity (within 2 m) to the injection location but were not directly located above the injectors (Fig. 3A). With time, and

as the injection rate increased, larger CH_4 effluxes and greater lateral migration were observed, with measurable effluxes up to 3 m from the injection location. Higher CH_4 effluxes were measured downgradient, as opposed to upgradient, of the injection point relative to the direction of groundwater flow, particularly with the highest injection rate in Phase 4 (Fig. 3A). The areal extent of CH_4 effluxes increased from 15 m^2 with maximum effluxes of 7.0 μmol m^{-2} s^{-1} (9.7 g CH_4 m^{-2} d^{-1}) in Phase 1 to 25 m^2 with effluxes up to 623.1 μmol m^{-2} s^{-1} (863.5 g CH_4 m^{-2} d^{-1}) in Phase 4. On the other hand, in Phase 3, CH_4 effluxes declined at all measurement locations and were highest upgradient of the injection location (10.1 μmol m^{-2} s^{-1} [14.0 g CH_4 m^{-2} d^{-1}]) (Fig. 3A). A similar observation was made with the survey measurement CO_2 effluxes, which increased from Phase 1 to Phase 2, with a greater lateral reach of elevated emissions approaching an areal extent of 25 m^2 (Fig. 3B). During Phase 4, the greatest CO_2 efflux was measured with the survey chamber (71.5 μmol m^{-2} s^{-1} [271.9 g CO_2 m^{-2} d^{-1}]) 1 m upgradient of the injection location (Fig. 3B).

The spatial distribution and evolution of surficial effluxes was supported by the observed soil gas concentrations. After the injection commenced, CH_4 concentrations within the vadose zone at a depth 50 cm had a similar spatial distribution to that of the corresponding surface effluxes (compare Fig. 3A and 4A). A CH_4 hot spot was observed in the vadose zone located adjacent to Chamber 2, 1 m offset from the injection location. As was observed for CH_4 effluxes, vadose zone CH_4 gas concentrations increased with greater injection rates and declined when
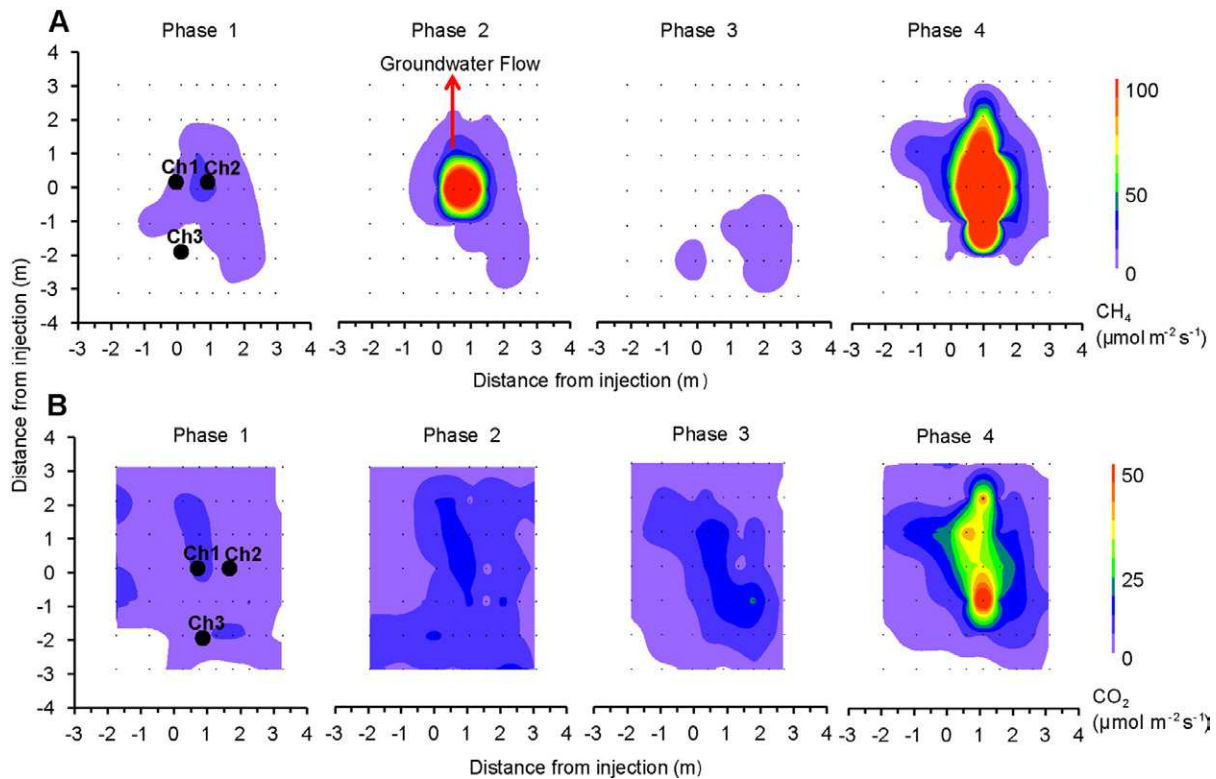
Fig. 3. Spatial distribution of (A) CH_4 effluxes and (B) CO_2 effluxes from Phases 1 to 4 taken with survey measurements on Day 27, 35, 70, and 72, respectively. Black points indicate survey measurement locations, and symbols denote the location of long-term chambers (Ch1, Ch2, and Ch3). The magnitude and spatial distribution of effluxes generally increased with greater injection rates.
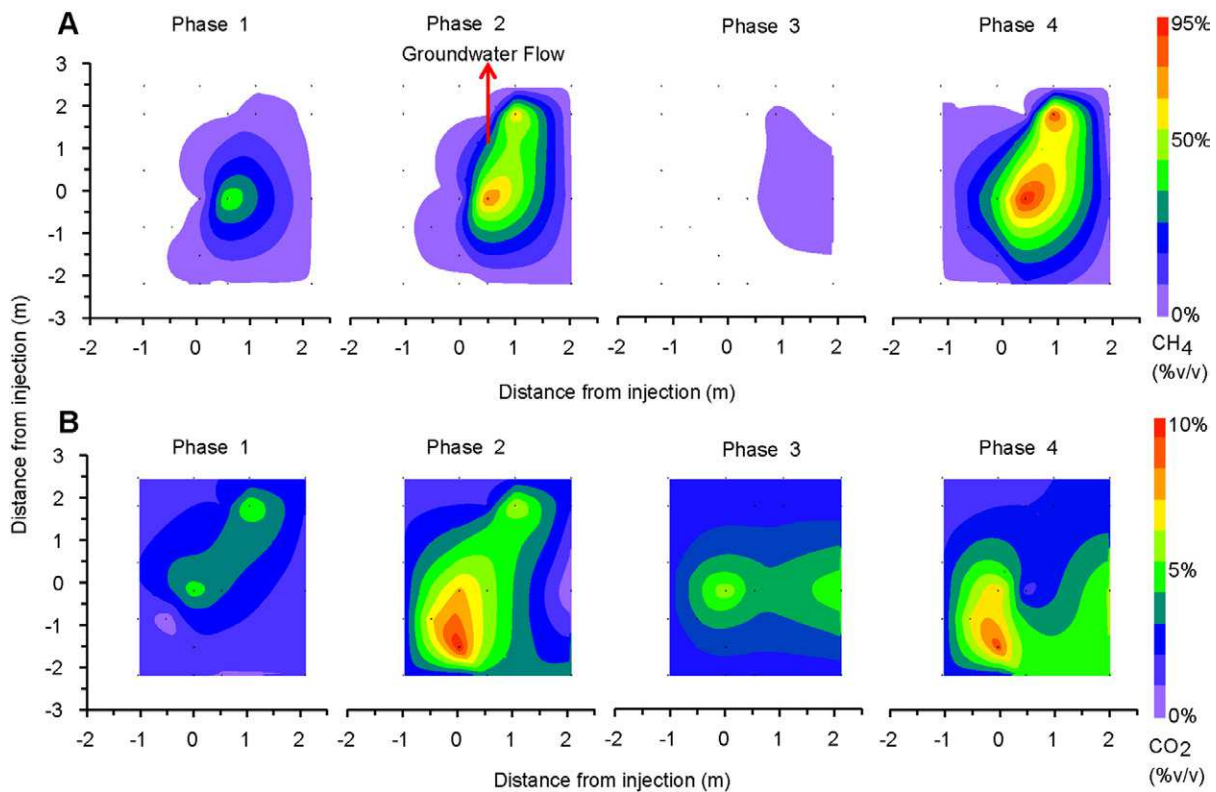

Fig. 4. Gas concentration (% v/v) at 50 cm depth from Phase 1, 2, 3, and 4 taken on Day 27, 35, 70, and 72, respectively, for (A) CH_4 and (B) CO_2. Black points indicate sampling locations for which samples were collected within an hour of each other over one sample round. Gas concentrations increased with greater injection rates.

the 4.5-m injector was turned off in Phase 3. During Phase 1, CH_4 concentrations reached 50% (v/v) within the hotspot and increased to >90% (v/v) during the highest injection rate (Phase 4). In Phase 3, CH_4 soil gas concentrations declined to <5% (v/v). Similar to the surficial effluxes, CH_4 soil gas concentrations increased preferentially in the direction of groundwater flow. In Phases 2 and 4, CH_4 concentrations >30% (v/v) were observed up to 2 m downgradient of the injection location (Fig. 4A). Concentrations of CO_2 soil gas at 50 cm depth also followed a similar spatial distribution to the effluxes, with higher concentrations along the center line and upgradient of the injection point relative to the groundwater flow direction (compare Fig. 3B and 4B). The spatial extent of the CO_2 soil gas plume grew during Phase 2 of the experiment, with concentrations up to 10% (v/v) observed up to 2 m away from the injection site. Concentrations of CO_2 within the CH_4 hotspot tended to be lower than those at the fringe of the hotspot. This was particularly observed during the highest injection rate when CO_2 was below 1% (v/v) at the CH_4 hotspot (Fig. 4B).

The fact that the highest CH_4 and CO_2 effluxes (at Chamber 2) were horizontally offset 1 m from the injection point further highlights that GM was affected by aquifer heterogeneities. The aquifer at the field site is known to consist of fine silt lenses that can result in preferential GM and lateral gas displacement (Tomlinson et al., 2003). The effects of soil heterogeneity on GM have also been reported by Delahaye and Pérez de Agreda (2002) and Esposito (2014) and in laboratory experiments (Chamindu Deepagoda et al., 2016). Increased CH_4 surface emissions and soil gas concentrations along the direction of groundwater flow (3 m downgradient) (Fig. 3A and 4A) suggest that free-phase CH_4 was "dragged" along with flowing groundwater and subsequently contributed to emissions. Over the duration of the experiment, CH_4 and CO_2

surface emissions and soil gas concentrations increased and extended 3 m downgradient of the injection location, confirming lateral gas displacement in the vadose zone (Fig. 3 and 4). Similar observations were made in the saturated zone where the highest injection rate (Phase 4) resulted in extensive dissolved CH_4 plumes at 2- and 6-m depths, reaching as far as 10 m from the injection location in the direction of groundwater flow (Cahill et al., 2018). Maxima both in terms of emissions and soil gas concentrations tended not to be colocated for CH_4 and CO_2, suggesting complex interactions between GM and CH_4 oxidation processes in the vadose zone.

Evolution of Gas Migration and Methane Oxidation Processes in the Vadose Zone

Stable carbon isotope values in CO_2 and CH_4 from a depth of 50 cm near Chambers 2 and 3 confirm the occurrence of CH_4 oxidation and indicate that oxidation began within the first 7 d of injection (Fig. 5). There was insufficient background CH_4 to determine its $\delta^{13}C$ value. The $\delta^{13}C$ value of the injected CH_4 was −42‰ and hence was markedly different from the carbon isotope ratios of biogenic CH_4. Background soil gas CO_2 had a $\delta^{13}C$ value of −24‰. Trends over time indicate an increase for $\delta^{13}C$-CH_4 in soil gas to values around −20‰, with $\delta^{13}C$-CO_2 values decreasing to below −40‰ near Chambers 2 and 3 (Fig. 5). Enrichment of ^{13}C in CH_4 and ^{12}C in CO_2 indicates microbial degradation of CH_4 due to the preferential utilization of CH_4 containing the light isotope (^{12}C) to produce CO_2 (Whiticar and Faber, 1986). This was particularly noticeable toward the end of Phase 2 at Chamber 2 when $\delta^{13}C$-CO_2 values became more negative. During the same period, a rise in CO_2 effluxes and a decline in CH_4 effluxes were observed at Chambers 1 and 2 (Fig. 2), consistent with accelerating microbially mediated CH_4 oxidation.

Correlating the isotopic data for CH_4 and CO_2 with the magnitude of CH_4 effluxes reveals that lower CH_4 effluxes to the atmosphere (0.01–10.0 $\mu mol\ m^{-2}\ s^{-1}$ [0.01–13.8 $g\ CH_4\ m^{-2}\ d^{-1}$])
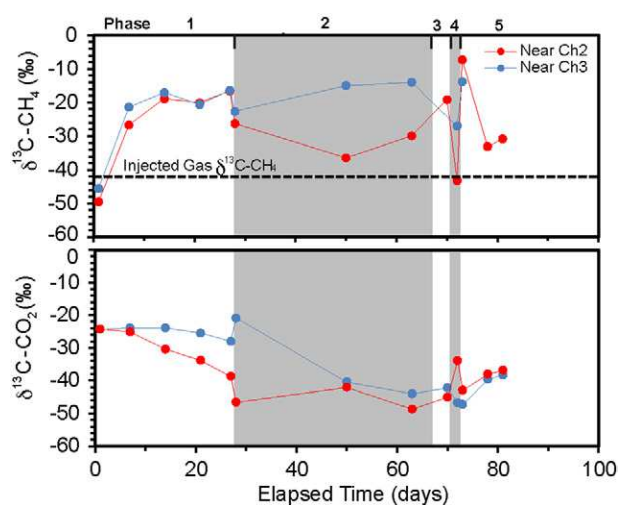

Fig. 5. Stable carbon isotopic composition (‰) at 50 cm depth measured over time near Chambers 2 and 3. The $\delta^{13}C$-CH_4 values increase beginning in Phase 1, whereas $\delta^{13}C$-CO_2 values decrease. Isotopic compositions are similar to the injected gas during the highest injection rate (Phase 4).
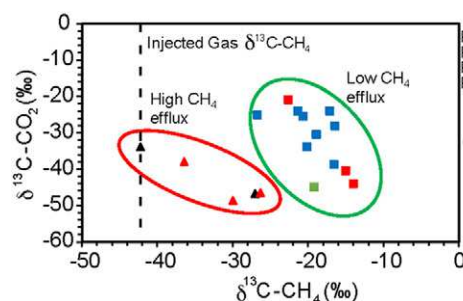

Fig. 6. Isotopic composition of soil gas samples collected at various locations at 50 cm depth throughout the experiment. Different CH_4 gas injection rates are indicated with respective colors for each phase. Methane effluxes measured at the surface prior to sampling are indicated by the shape, where squares represent effluxes between 0.01 and 10 $\mu mol\ m^{-2}\ s^{-1}$ and triangles indicate effluxes >10 $\mu mol\ m^{-2}\ s^{-1}$. Advective gas migration is evident with higher CH_4 effluxes during Phase 2 and in Phase 4.

are synonymous with greater progression of aerobic CH_4 oxidation, whereas higher CH_4 effluxes show CH_4 signatures closer to the isotopic composition of the injected CH_4. However, samples from high-efflux events still show substantial enrichment of ^{12}C-CO_2, indicating that CH_4 oxidation is occurring (Fig. 6). This observation implies that CH_4 oxidation capacity is limited and that under high-flux conditions only a relatively small fraction of CH_4 released into the vadose zone is oxidized prior to arrival at the ground surface.

Baseline soil gas concentrations measured 2 d prior to commencing injection showed that CH_4 concentrations were nondetectable, CO_2 ranged from 2 to 3% (v/v), O_2 ranged from 17 to 19% (v/v), and N_2 ranged from 78 to 79% (v/v) across all locations. From Phase 1 to Phase 2, N_2, CH_4, and CO_2 increased and O_2 decreased near Chambers 1 and 3 (Fig. 7). A rise in CO_2 concentrations supports increasing rates of CH_4 oxidation, which were most visible for gas samples collected near Chamber 3. The decline in partial pressures of CH_4 and O_2 due to CH_4 oxidation causes downward advective gas transport into the soil, leading to increased N_2 gas concentrations. Similar observations have been made at a crude oil spill site (Amos et al., 2005; Molins and Mayer, 2007; Revesz et al., 1995). Evidence for downward advection into the reaction zone is most visible during the early stage of Phase 2 (near Chamber 1) and throughout Phase 2 near Chamber 3 (Fig. 7). On the other hand, Amos et al. (2005) also showed that depletion of N_2 in the vadose zone is indicative of upward advective gas transport, here caused by the displacement of soil gas by the injected CH_4. Such conditions are clearly visible in most soil gas samples near Chamber 2, during the latter part of Phase

2 near Chamber 1, and at all sampling locations during the period with the highest injection rate (Phase 4) (Fig. 7).

Reactive transport modeling was used to further help delineate the governing transport processes and biogeochemical reactions. The model was constrained by data from Chamber 2 for a low-flux event that occurred on Day 28 (Phase 2) during the lowest injection rate and for a high-flux event that occurred on Day 72 during the highest injection rate (Phase 4). For both scenarios, model results were compared with the gas composition (% v/v) and stable C isotope ratios ($^{13}C/^{12}C$) of CO_2 and CH_4 from samples collected near Chamber 2 at depths of 10, 30, and 50 cm as well as with CH_4 and CO_2 effluxes measured at Chamber 2. Good agreement between simulated and observed results was obtained for both high- and low-flux conditions (Fig. 8 and 9).

In the high-flux simulation, CH_4 concentrations were elevated below a depth of 30 cm, whereas N_2 and O_2 were strongly depleted. Above 30 cm depth, the coexistence of O_2 and CH_4 provided conditions favorable for aerobic CH_4 oxidation, leading to maximum CO_2 concentrations at a depth of 20 cm (Fig. 8A). Values for $\delta^{13}C$-CH_4 remained relatively unchanged in comparison to the injected gas (−42‰), especially in the lower portion of the soil profile, where $\delta^{13}C$-CO_2 values were close to the background value (−24‰). In the upper portion of the soil profile, $\delta^{13}C$-CO_2 decreased to values of less than −40‰, whereas soil gas CH_4 became progressively enriched in ^{13}C (Fig. 9A). These results indicate aerobic CH_4 oxidation in the upper 50 cm of the soil profile but with a limited impact on the isotopic composition of CH_4 due to its high abundance, consistent with data shown in Fig. 6. In addition, the simulations confirm that diffusive O_2 influxes were partially offset by advective O_2 effluxes and limited overall O_2 ingress and consequently CH_4 degradation (Fig. 10A). Model results also indicate that, for high-flux conditions, CH_4 and CO_2 fluxes were predominantly advective up to ~10 cm below the ground surface (Fig. 10A). In this region, a transition to a diffusion-dominated transport regime takes place and persists to the top of the soil column. The modeling supports the results and interpretations discussed above based on gas composition, efflux, and isotopic data.

Under low-flux conditions, CH_4 concentrations were lower than for high-flux conditions throughout most of the soil profile, particularly in the upper 30 cm. Conversely, O_2 concentrations penetrated deeper into the vadose zone, extending the region of active aerobic CH_4 oxidation to a greater depth and resulting in higher CO_2 concentrations at 20 cm (Fig. 8B). Values for $\delta^{13}C$-CH_4 increased, providing direct evidence for CH_4 oxidation (Fig. 9B). These results also suggest active aerobic oxidation of CH_4 in the upper 60 cm of the soil column. In the simulations, the carbon isotope ratios of CO_2 near the ground surface are affected by the process of root and soil respiration, explaining the return to less negative $\delta^{13}C$ values (Fig. 9B). For low-flux conditions, advective CH_4 transport in the soil column is restricted to the lower part of the soil column and ends at a depth of ~45 cm, where fluxes become predominantly diffusive (Fig. 10B). The simulations also show that diffusive N_2 influxes were balanced by advective and nonequimolar (not shown) effluxes (Fig. 10B). Under low-flux
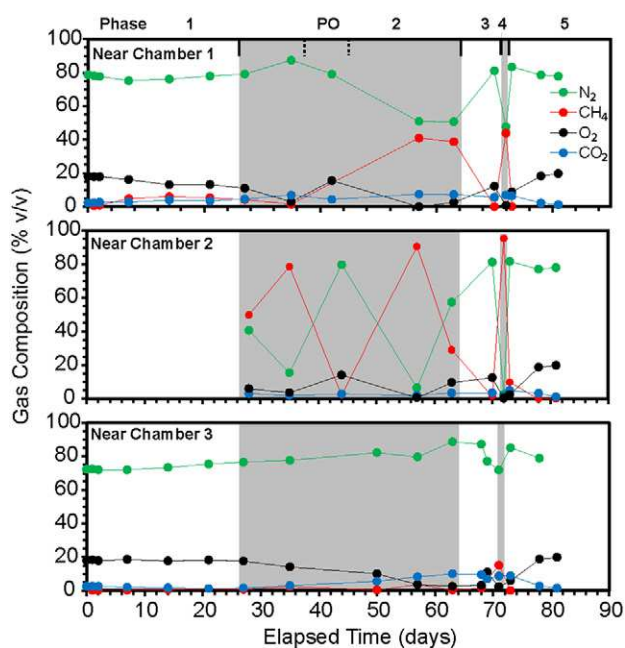

Fig. 7. Gas concentration (% v/v) over time measured at 50 cm depth near Chambers 1, 2, and 3. Methane concentrations increased with time, except during the power outage (PO) during Phase 2.
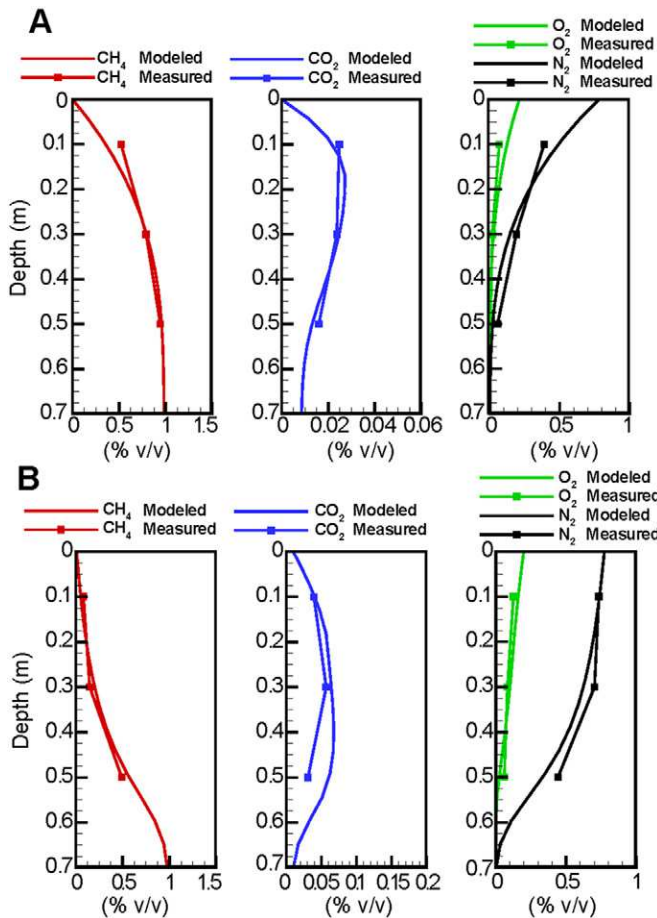
Fig. 8. Modeled and measured gas concentration profiles for (A) high and (B) low CH$_4$ flux conditions. Higher CH$_4$ concentrations with depleted N$_2$ concentrations are indicative of advective gas migration for the high-flux simulation. In contrast, lower CH$_4$ concentrations and larger N$_2$ concentrations are indicative of a more diffusion-dominated transport regime.

Fig. 9. Modeled and measured δ^{13}C values of CH$_4$ and CO$_2$ (in ‰) for (A) high and (B) low CH$_4$ flux conditions. High fluxes result in minimal change to δ^{13}C-CH$_4$ values in comparison to the injected gas. In contrast, the remaining CH$_4$ became enriched in ^{13}C during the low-flux simulation, indicating degradation.

conditions, the results suggest that O$_2$ ingress was diffusion dominated with limited upward advection (Fig. 10B). These observations explain the greater depth of O$_2$ ingress under low-flux conditions in comparison to the high-flux case. Reactive transport modeling results further confirm that periods of low CH$_4$ effluxes allowed atmospheric O$_2$ to diffuse deeper into the soil column and promote greater and more complete oxidation of CH$_4$.

Volumetric Water Content and Barometric Pressure

Volumetric water content in the vadose zone averaged ∼20%, with a few events where moisture contents temporarily increased after precipitation events. Barometric pressure fluctuated during the experiment between 97 and 101 kPa. Previous studies have indicated that these parameters can either enhance (Kim et al., 2012; Rey et al., 2017; Xu et al., 2014) or inhibit (Castro et al., 1995; Scheutz and Kjeldsen, 2004) GM to the surface and surface gas effluxes. Attempts to associate variations in moisture contents and barometric pressure to the episodic nature of the observed effluxes were
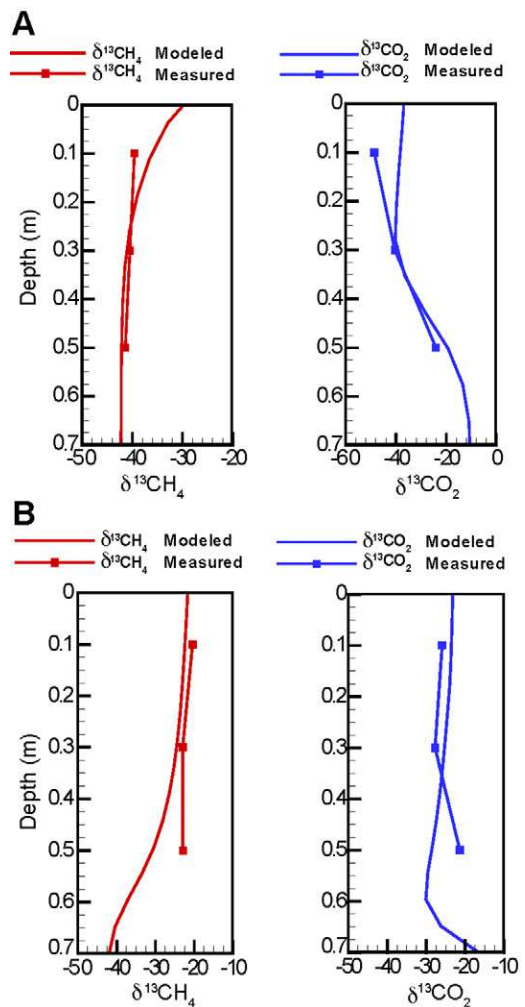
not successful (not shown), suggesting that at this site subsurface processes controlled temporal evolution of the effluxes to a greater degree than VWC in the vadose zone and barometric pressure fluctuations. The limited thickness of the vadose zone and the relatively longer GM pathway through the saturated zone likely explain the lack of correlation of efflux data with atmospheric and vadose zone parameters.

Fraction of Injected Methane Lost from the Saturated Zone and Emitted to the Atmosphere as Methane

Mass balance calculations (see Supplemental Material for approach) indicate that, over 75 d of the experiment, ∼30% of the injected CH$_4$ was emitted from the soil surface to the atmosphere as CH$_4$ effluxes (i.e., 12.2–15.3 m^3 compared with 51 m^3 injected). In Phase 1, a gradual increase in CH$_4$ effluxes was observed across all three long-term chambers until Day 26. Up to Day 26 ∼26% of the total injected gas was emitted at the soil
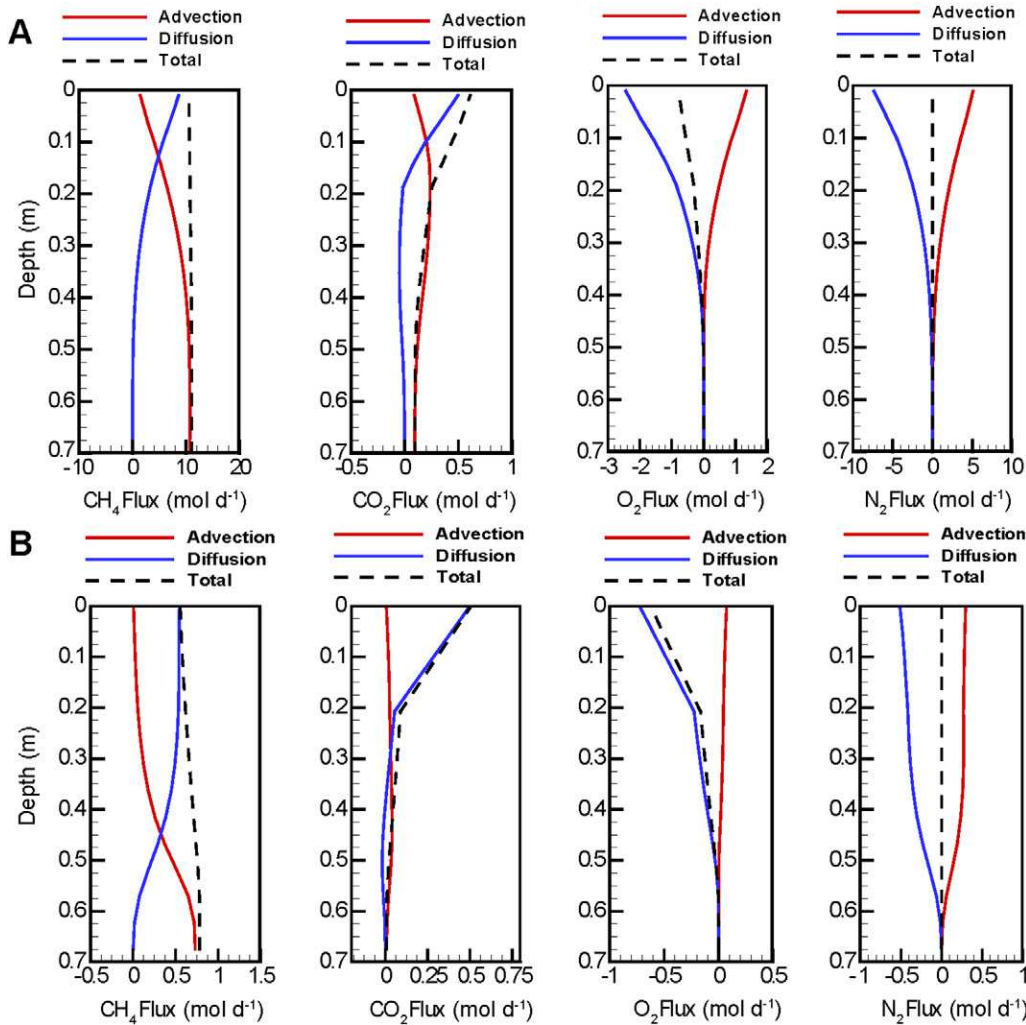
Fig. 10. Modeled CH_4, CO_2, O_2, and N_2 fluxes for (A) high and (B) low CH_4 flux conditions. Advection is the dominant transport mechanism for CH_4 and CO_2 up to ~10 cm for high-flux conditions. For low-flux conditions, diffusion becomes dominant for CH_4 at 45 cm. Fluxes of CO_2 were dominated by the contributions of root respiration above a depth of 20 cm. Diffusive O_2 and N_2 influxes are counteracted by advective effluxes. For low-flux conditions, O_2 influxes are dominated by diffusion driven by root respiration and CH_4 oxidation.

surface to the atmosphere. However, on Day 26 alone, 72% of the gas injected on that day was emitted to the atmosphere. This likely represents the effect of gas entrapment in the saturated zone and pressure build-up prior to a sudden release. A similar effect was observed during Phase 2, with additional occurrences of episodic effluxes due to the higher injection rates and thus greater pressure forces for CH_4 gas to overcome capillary forces. Approximately 38% of the gas injected during Phase 2 was emitted from the soil surface to the atmosphere as CH_4 effluxes. Significant mass loss events can be identified when examining the cumulative mass release of CH_4 at the ground surface (Fig. 11). Mass loss on the day of episodic efflux events ranged from 38 to 261% of the gas injected that day. Methane loss greater than the injected mass on that day suggests that some of the injected CH_4 remained trapped below the surface until buoyancy forces were great enough to overcome capillary forces, resulting in a rapid cumulative release of gas. During Phase 3, only ~15% of the injected gas (from 9 m depth) was emitted from the soil surface to the atmosphere. However, the CH_4 effluxes measured could also be a result of the release of residual CH_4 gas injected earlier, not necessarily corresponding to emissions directly related to the active injection at 9 m depth. In Phase 4, 41% of the mass injected was lost to the atmosphere as CH_4. The greater total CH_4 loss in each phase corresponds with

the increasing injection rates. However, the episodic high mass loss events within each phase also demonstrate that efflux at surface does not necessarily directly correspond to the magnitude of subsurface leakage.

Background CO_2 effluxes were too variable to reliably quantify the mass of injected CH_4 lost and emitted as CO_2. However, rising CO_2 effluxes above background levels at all three chambers further confirm that some CH_4 was also lost to aerobic oxidation, yielding CO_2 as a product. In this context, the mass of dissolved CO_2 and other carbonate species retained in vadose zone pore water, expected in the presence of increased CO_2 partial gas pressures in soil gas, has been neglected, implying that the increase of CH_4 oxidation rates may be even more significant than inferred from the increasing CO_2 effluxes alone. Average CO_2 effluxes were greatest in Phase 2 (Table 4), suggesting that the microbial community had fully developed and that there was sufficient CH_4 and O_2 to drive methanotrophic oxidation of CH_4. The cumulative mass of CO_2 emitted was greater than CH_4 emitted at Chambers 1 and 3, indicating that regions with lower CH_4 fluxes had relatively greater CH_4 loss to degradation (Fig. 11), consistent with the isotopic results (Fig. 6). Cumulative mass loss for CH_4 demonstrates that the episodic effluxes in Phase 2 and the high injection rate in Phase 4 resulted in significant,
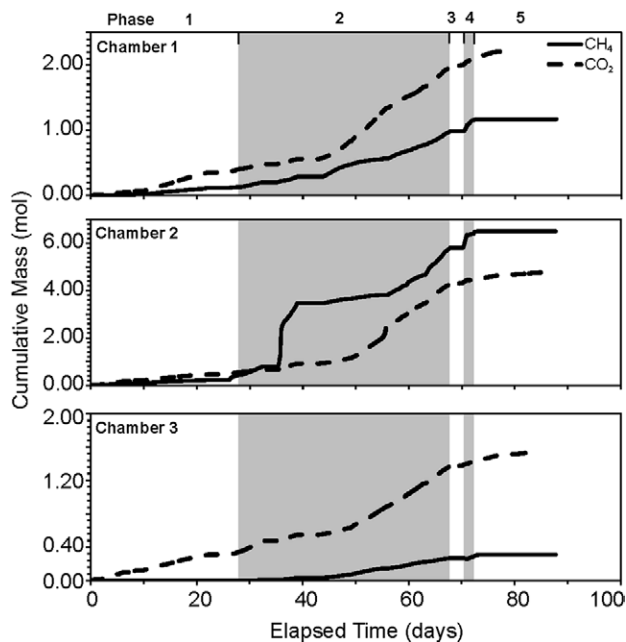
Fig. 11. Cumulative mass of CH_4 and CO_2 emitted over time for Chambers 1, 2, and 3. Episodic events during Phase 2 and in response to the high injection rate during Phase 4 resulted in significant CH_4 emissions. Greater CO_2 emissions at Chambers 1 and 3 are indicative of CH_4 oxidation.

yet short-lived, CH_4 emission events from the soil surface to the atmosphere (Fig. 11). In contrast, low fluxes allowed for a greater mass of CO_2 to be released through CH_4 oxidation. These trends are also supported by the RTM results, where high CH_4 fluxes resulted in limited CH_4 oxidation compared with low fluxes (Table 5).

In general, the method used to estimate the total CH_4 lost to the atmosphere (30%) does not account for losses due to oxidation and emissions as CO_2. It is likely that a significant portion of CH_4 was lost to oxidation, as indicated by the changes in stable carbon isotopes and the rise in CO_2 effluxes, particularly in Phase 2. Neglecting the emissions of CO_2 generated by CH_4 oxidation implies that the 30% estimate reported here may be conservative. However, the uncertainties associated with the mass balance estimate are substantial due to the small number of long-term chambers, the limited number of spatial surveys, and the assumption that measured CH_4 effluxes are representative of an area larger than that directly covered by the collar (see Methods in the Supplemental Material). The mass balance results must therefore be considered qualitative in nature.

Conceptual Model and Implications for Monitoring and Detecting Fugitive Methane

The experimental results demonstrate that subsurface gas leakage can result in spatially distributed and intermittent GM to the vadose zone, where both diffusion and advection contribute to CH_4 transport (Fig. 12). Advection is more likely to dominate under higher leakage rates (i.e., compare Phase 1
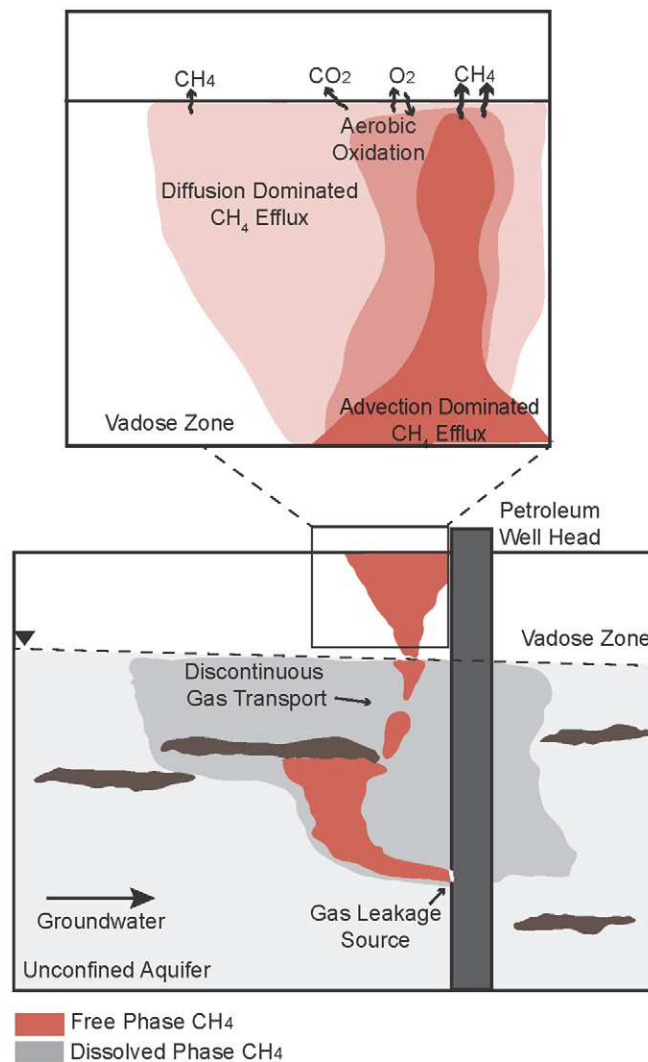

Fig. 12. Conceptual model of the fate of fugitive CH_4 in an unconfined aquifer and its overlying vadose zone. Free-phase CH_4 migrates vertically into the vadose zone along preferential pathways. At the base of the vadose zone, CH_4 migration is dominated by advective transport, resulting in higher CH_4 effluxes to the atmosphere above the source point. Methane undergoes aerobic oxidation as it migrates further from the source point, resulting in lower effluxes to the atmosphere dominated by diffusive transport.

with Phase 4) and where preferential pathways have formed (i.e., compare Chamber 2 with Chamber 3). Advection-dominated gas transport may lead to less complete CH_4 oxidation and result in larger CH_4 emissions at the surface. Diffusion-dominated transport tends to lead to more complete CH_4 oxidation, resulting in enhanced CO_2 emissions (Fig. 12). The episodic nature and complex spatial distribution of effluxes suggests that continuous long-term monitoring at multiple locations is needed to evaluate the occurrence and potential risks of fugitive CH_4 migration on oil and gas well pads.

The spatial distributions of CH_4 and CO_2 effluxes in this experiment were relatively contained in a 25-m^2 area (up to 3 m from the injection point) and increased with greater injection rates. However, the extent of lateral GM did not reach as far as the

Table 5. Mass balance results for low and high CH_4 flux simulations.

Parameter	Low flux		High flux	
	CH_4	CO_2	CH_4	CO_2
	———— μmol m^{-2} s^{-1} ————			
Measured				
Efflux	2.43	7.41	106.94	6.83
Modeled				
C source from injection and root respiration	6.71	3.36	113.89	4.05
C loss to gas phase	−4.86	−4.28	−107.75	−7.06
C source or loss from oxidation	−1.74	0.93	−6.13	3.01
Diffusive efflux	4.86	4.28	94.44	6.13
Advective efflux	0.00	0.00	13.19	0.91
C loss to storage gas phase	0.00	0.00	0.00	0.00

groundwater CH_4 plume in the saturated zone (3 vs. 10 m down-gradient of the injection location in the direction of groundwater flow) (Cahill et al., 2018; Steelman et al., 2017), suggesting that near-surface measurements may not capture the spatial extent and impact of fugitive gas releases on freshwater aquifers. This study demonstrated that subtle heterogeneities can have a significant impact on GM. It can be expected that greater lateral GM would occur in more heterogeneous media and for natural gas releases at greater depths. In addition, the vadose zone at this site was relatively thin (<1 m); in a deeper vadose zone, larger vertical distances to the ground surface could result in greater residence times for CH_4 gas. This could lead to a delayed response in effluxes at the surface, more lateral spreading, and greater CH_4 oxidation if O_2 can be supplied to depth.

Conclusions

Monitoring of a controlled natural gas release into a shallow unconfined aquifer provided the opportunity to evaluate the pathways and mechanisms of vadose zone GM and surface emissions. Results demonstrate that surficial CH_4 and CO_2 effluxes were strongly influenced by the rate of gas release into the aquifer and subsurface heterogeneity. Higher injection rates led to greater average CH_4 effluxes and lateral migration. As the injection rate increased, CH_4 migrated 3 m from the injection location and affected an area approaching 25 m^2. Despite continuous injection rates, effluxes were episodic in nature and varied in magnitude over time (e.g., CH_4 effluxes ranged from 1.2 to 2679 μmol m^{-2} s^{-1} [1.7–3713 g CH_4 m^{-2} d^{-1}] at Chamber 2 in Phase 2). Temporal and spatial monitoring and RTM demonstrated that high CH_4 effluxes were governed by advective GM (Fig. 12). In contrast, low CH_4 efflux conditions were dominated by diffusive GM allowing for greater O_2 ingress and more complete CH_4 oxidation (Fig. 12). The increasing CO_2 effluxes and the change of carbon isotope ratios of CH_4 and CO_2 indicated that there was a strong propensity for CH_4 oxidation

in the vadose zone. This observation suggests that significant amounts of the injected CH_4 were lost to oxidation and emitted to the atmosphere as CO_2. The mass loss to the atmosphere is likely greater than what has been accounted for solely based on CH_4 effluxes ($\sim$30%). Our results demonstrate that, even in a relatively homogenous aquifer, subtle heterogeneities can lead to preferential pathways that influence the spatial and temporal distribution of CH_4 and CO_2 effluxes at the ground surface. Effluxes were found to be episodic and resulted in large, yet short-lived emissions of CH_4. In addition, localized hot spots led to subsurface CH_4 concentrations that reached high concentrations above the lower explosive limit (5% v/v) and in some cases exceeded 90% (v/v) CH_4 close to the ground surface.

These results allowed us to develop a conceptual model of fugitive CH_4 migration from the vadose to the ground surface (Fig. 12). Although recent research has focused on fugitive CH_4 impacts in the saturated zone and atmosphere, few studies have quantified and assessed migration from the saturated zone to the ground surface. Our conceptual model will help to inform monitoring of fugitive gas from oil and gas wells. The results demonstrate the need for subsurface characterization followed by continuous and spatially discrete monitoring from the aquifer to the ground surface to detect and quantify fugitive GM.

References

Allen, D.T., V.M. Torres, J. Thomas, D.W. Sullivan, M. Harrison, A. Hendler, et al. 2013. Measurements of methane emissions at natural gas production sites in the United States. Proc. Natl. Acad. Sci. 110:17768–17773. doi:10.1073/pnas.1304880110

Allen-King, R.M., R.M. Halket, D.R. Gaylord, and M.J.L. Robin. 1998. Characterizing the heterogeneity and correlation of perchloroethene sorption and hydraulic conductivity using a facies-based approach. Water Resour. Res. 34:385–396. doi:10.1029/97WR03496

Alm, J., N.J. Shurpali, M. Maljanen, E.-S. Tuittila, K. Minkkinen, T. Laurila, and S. Saarnio. 2007. Methods for determining emission factors for the use of peat and peatlands: Flux measurements and modelling. Boreal Environ. Res. 12:85–100.

Amos, R.T., K.U. Mayer, B.A. Bekins, G.N. Delin, and R.L. Williams. 2005. Use of dissolved and vapor-phase gases to investigate methanogenic degradation of petroleum hydrocarbon contamination in the subsurface. Water Resour. Res. 41:W02001. doi:10.1029/2004WR003433

Bachu, S. 2017. Analysis of gas leakage occurrence along wells in Alberta, Canada, from a GHG perspective: Gas migration outside well casing. Int. J. Greenhouse Gas Control 61:146–154 . doi:10.1016/j.ijggc.2017.04.003

Baird, A.J., C.W. Beckwith, S. Waldron, and J.M. Waddington. 2004. Ebullition of methane-containing gas bubbles from near-surface *Sphagnum* peat. Geophys. Res. Lett. 31:L21505. doi:10.1029/2004GL021157

Bird, M.I., and P. Pousai. 1997. Variations of d^{13}C in the surface soil organic carbon pool. Global Biogeochem. Cycles 11:313–322. doi:10.1029/97GB01197

Bogner, J.E., K.A. Spokas, and E.A. Burton. 1997. Kinetics of methane oxidation in a landfill cover soil: Temporal variations, a whole-landfill oxidation experiment, and modeling of net CH_4 emissions. Environ.

Sci. Technol. 31:2504–2514 . doi:10.1021/es960909a

Boothroyd, I.M., S. Almond, S.M. Qassim, F. Worrall, and R.J. Davies. 2016. Fugitive emissions of methane from abandoned, decom-missioned oil and gas wells. Sci. Total Environ. 547:461–469. doi:10.1016/j.scitotenv.2015.12.096

Cahill, A.G., B.L. Parker, B. Mayer, K.U. Mayer, and J.A. Cherry. 2018. High resolution spatial and temporal evolution of dissolved gases in groundwater during a controlled natural gas release experiment. Sci. Total Environ. 622–623:1178–1192. doi:10.1016/j.scitotenv.2017.12.049

Cahill, A.G., C.M. Steelman, O. Forde, O. Kuloyo, S.E. Ruff, B. Mayer, et al. 2017. Mobility and persistence of methane in groundwater in a controlled-release field experiment. Nat. Geosci. 10:289–294. doi:10.1038/ngeo2919

Castro, M.S., P.A. Steudler, J.M. Melillo, J.D. Aber, and R.D. Bowden. 1995. Factors controlling atmospheric methane consumption by temperate forest soils. Global Biogeochem. Cycles 9:1–10. doi:10.1029/94GB02651

Caulton, D.R., P.B. Shepson, R.L. Santoro, J.P. Sparks, R.W. Howarth, A.R. In-graffea, et al. 2014. Toward a better understanding and quantification of methane emissions from shale gas development. Proc. Natl. Acad. Sci. 111:6237–6242. doi:10.1073/pnas.1316546111

Council of Canadian Academies. 2014. Environmental impacts of shale gas extraction in Canada. Expert Panel on Harnessing Science and Technology to Understand the Environmental Impacts of Shale Gas Extraction, Council of Canadian Academies, Ottawa, ON.

Chamindu Deepagoda, T.K.K., K.M. Smits, and C.M. Oldenburg. 2016. Effect of subsurface soil moisture variability and atmospheric conditions on methane gas migration in shallow subsurface. Int. J. Greenhouse Gas Control 55:105–117. doi:10.1016/j.ijggc.2016.10.016

Dai, J., Y. Ni, D. Gong, Z. Feng, D. Liu, W. Peng, and W. Han. 2017. Geochemi-cal characteristics of gases from the largest tight sand gas field (Sulige) and shale gas field (Fuling) in China. Mar. Pet. Geol. 79:426–438. doi:10.1016/j.marpetgeo.2016.10.021

Darrah, T.H., A. Vengosh, R.B. Jackson, N.R. Warner, and R.J. Poreda. 2014. Noble gases identify the mechanisms of fugitive gas contamination in drinking-water wells overlying the Marcellus and Barnett Shales. Proc. Natl. Acad. Sci. 111:14076–14081. doi:10.1073/pnas.1322107111

Davies, R.J., S. Almond, R.S. Ward, R.B. Jackson, C. Adams, F. Worrall, et al. 2014. Oil and gas wells and their integrity: Implications for shale and unconventional resource exploitation. Mar. Pet. Geol. 56:239–254. https://doi.org/10.1016/j.marpetgeo.2014.03.001

Delahaye, C.H., and E.A. Pérez de Agreda. 2002. Soil heterogene-ity and preferential paths for gas migration. Eng. Geol. 64(2). doi:10.1016/S0013-7952(01)00104-1

Dusseault, M., M. Gray, and P. Nawrocki. 2000. Why oilwells leak: Cement behavior and long-term consequences. In: International Oil and Gas Conference and Exhibition in China, Beijing. 7–10 Nov. 2000. Soc. Pet. Eng., Richardson, TX. doi:10.2118/64733-MS

Dusseault, M., and R. Jackson. 2014. Seepage pathway assessment for natural gas to shallow groundwater during well stimulation, in production, and after abandonment. Environ. Geosci. 21(3):107–126. doi:10.1306/eg.04231414004

Erno, B., and R. Schmitz. 1996. Measurements of soil gas migration around oil and gas wells in the Lloydminster area. J. Can. Pet. Technol. 35(7). doi:10.2118/96-07-05

Esposito, A. 2014. Migration of natural gas through heterogeneous sandy soils affected by atmospheric boundary conditions. In: Unconventional Resources Technology Conference, Denver, CO. 25–27 Aug. 2014. Aust. Soc. Exploration Geophys., NSW, Australia. doi:10.15530/urtec-2014-1937753

Ferbey, T., A.S. Hickin, T.E. Demchuck, and V.M. Levson. 2008. Northeast British Columbia Aggregate Mapping Program: A summary of selected aggregate occurrences northeast of Fort Nelson. Ministry of Energy and Mines, Vancouver, BC, Canada.

Forbrich, I., L. Kutzbach, A. Hormann, and M. Wilmking. 2010. A compari-son of linear and exponential regression for estimating diffusive CH_4 fluxes by closed-chambers in peatlands. Soil Biol. Biochem. 42:507–515. doi:10.1016/j.soilbio.2009.12.004

Golding, S.D., C.J. Boreham, and J.S. Esterle. 2013. Stable isotope geo-

chemistry of coal bed and shale gas and related production waters: A review. Int. J. Coal Geol. 120:24–40. doi:10.1016/j.coal.2013.09.001

Gorody, A.W. 2012. Factors affecting the variability of stray gas concentra-tion and composition in groundwater. Environ. Geosci. 19(1):17–31. doi:10.1306/eg.12081111013

Hammond, P.A. 2015. The relationship between methane migration and shale-gas well operations near Dimock, Pennsylvania, USA. Hydrogeol. J. 24:503–519. doi:10.1007/s10040-015-1332-4

Harrison, S.S. 1983. Evaluating system for ground-water contamination hazards due to gas-well drilling on the glaciated Appalachian plateau. Ground Water 21:689–700. doi:10.1111/j.1745-6584.1983.tb01940.x

Harrison, S.S. 1985. Contamination of aquifers by overpressur-ing the annulus of oil and gas wells. Ground Water 23:317–324. doi:10.1111/j.1745-6584.1985.tb00775.x

Heijmans, M.M., P.D. Arp, and F.S. Chapin. 2004. Carbon dioxide and water vapour exchange from understory species in boreal forest. Agric. For. Meteorol. 123(3):135–147. doi:10.1016/j.agrformet.2003.12.006

Humez, P., B. Mayer, J. Ing, M. Nightingale, V. Becker, A. Kingston, et al. 2016. Occurrence and origin of methane in groundwater in Alberta (Canada): Gas geochemical and isotopic approaches. Sci. Total Environ. 541:1253–1268. doi:10.1016/j.scitotenv.2015.09.055

Jackson, R.B., A. Vengosh, J.W. Carey, R.J. Davies, T.H. Darrah, F. O'Sullivan, and G. Pétron. 2014. The environmental costs and benefits of fracking. Annu. Rev. Environ. Resour. 39:327–362. doi:10.1146/annurev-environ-031113-144051

Jackson, R.B., A. Vengosh, T.H. Darrah, N.R. Warner, A. Down, R.J. Poreda, et al. 2013. Increased stray gas abundance in a subset of drinking water wells near Marcellus shale gas extraction. Proc. Natl. Acad. Sci. 110:11250–11255. doi:10.1073/pnas.1221635110

Johnson, M.R., D.R. Tyner, S. Conley, S. Schwietzke, and D. Zavala-Araiza. 2017. Comparisons of airborne measurements and inventory estimates of methane emissions in the Alberta up-stream oil and gas sector. Environ. Sci. Technol. 51:13008–13017. doi:10.1021/acs.est.7b03525

Johnson, R.L., P.C. Johnson, D.B. McWhorter, R.E. Hinchee, and I. Goodman. 1993. An overview of in situ air sparging. Groundwater Monit. Rem. 13:127–135. doi:10.1111/j.1745-6592.1993.tb00456.x

Kang, M., S. Christian, M.A. Celia, D.L. Mauzerall, M. Bill, A.R. Miller, et al. 2016. Identification and characterization of high methane-emitting abandoned oil and gas wells. Proc. Natl. Acad. Sci. 113:13636–13641. doi:10.1073/pnas.1605913113

Kim, D.-G., R. Vargas, B. Bond-Lamberty, and M.R. Turetsky. 2012. Effects of soil rewetting and thawing on soil gas fluxes: A review of cur-rent literature and suggestions for future research. Biogeosciences 9:2459–2483. doi:10.5194/bg-9-2459-2012

Lan, X., R. Talbot, P. Laine, and A. Torres. 2015. Characterizing fugitive methane emissions in the Barnett Shale area using a mobile labora-tory. Environ. Sci. Technol. 49:8139–8146. doi:10.1021/es5063055

Law, B.E., F.M. Kelliher, D.D. Baldocchi, P.M. Anthoni, J. Irvine, D. Moore, and S. Van Tuyl. 2001. Spatial and temporal variation in respiration in a young ponderosa pine forest during a summer drought. Agric. For. Meteorol. 110:27–43. doi:10.1016/S0168-1923(01)00279-9

LI-COR. 2015. LI-8100A Automated soil CO_2 flux system & LI-8150 multi-plexer instruction manual. LI-COR, Lincoln, NE.

Mason, E.A., and A.P. Malinauskas. 1983. Gas transport in porous media: The dusty-gas model. Elsevier, Amsterdam.

McCray, J.E., and R.W. Falta. 1996. Defining the air sparging radius of influence for groundwater remediation. J. Contam. Hydrol. 24:25–52. doi:10.1016/0169-7722(96)00005-8

Millington, R.J. 1959. Gas diffusion in porous media. Science 130:100–102. doi:10.1126/science.130.3367.100-a

Molins, S., and K.U. Mayer. 2007. Coupling between geochemical reactions and multicomponent gas and solute transport in unsaturated media: A reactive transport modeling study. Water Resour. Res. 43:W05435. doi:10.1029/2006WR005206

Molins, S., K.U. Mayer, C. Scheutz, and P. Kjeldsen. 2008. Transport and re-action processes affecting the attenuation of landfill gas in cover soils. J. Environ. Qual. 37:459–468. doi:10.2134/jeq2007.0250

Molins, S., K.U. Mayer, R.T. Amos, and B.A. Bekins. 2010. Vadose zone attenuation of organic compounds at a crude oil spill site: Interactions between biogeochemical reactions and multicomponent gas transport. J. Contam. Hydrol. 112:15–29. doi:10.1016/j.jconhyd.2009.09.002

Mumford, K.G., J.E. Smith, and S.E. Dickson. 2010. The effect of spontaneous gas expansion and mobilization on the aqueous-phase concentrations above a dense non-aqueous phase liquid pool. Adv. Water Resour. 33:504–513. doi:10.1016/j.advwatres.2010.02.002

Myhre, G.D., F.M. Shindell, and W. Breon. 2013. Anthropogenic and natural radiative forcing. In: T.F. Stocker et al., editors, Climate change 2013: The physical science basis. Working Group I Contribution to the Fifth Assessment Report of the Intergovernmental Panel on Climate Change. Cambridge Univ. Press, Cambridge, UK. p. 659–740. doi:10.1017/CBO9781107415324.018

Nowamooz, A., J.-M. Lemieux, J. Molson, and R. Therrien. 2015. Numerical investigation of methane and formation fluid leakage along the casing of a decommissioned shale gas well. Water Resour. Res. 51:4592–4622. doi:10.1002/2014WR016146

Osborn, S.G., A. Vengosh, N.R. Warner, and R.B. Jackson. 2011. Methane contamination of drinking water accompanying gas-well drilling and hydraulic fracturing. Proc. Natl. Acad. Sci. 108:8172–8176. doi:10.1073/pnas.1100682108

Pihlatie, M.K., J.R. Christiansen, H. Aaltonen, J.F.J. Korhonen, A. Nordbo, T. Rasilo, et al. 2013. Comparison of static chambers to measure CH_4 emissions from soils. Agric. For. Meteorol. 171–172:124–136. doi:10.1016/j.agrformet.2012.11.008

Revesz, K., T.B. Coplen, M.J. Baedecker, P.D. Glynn, and M. Hult. 1995. Methane production and consumption monitored by stable H and C isotope ratios at a crude oil spill site, Bemidji, Minnesota. Appl. Geochem. 10:505–516. doi:10.1016/0883-2927(95)00021-6

Rey, A., C. Oyonarte, T. Morán-López, J. Raimundo, and E. Pegoraro. 2017. Changes in soil moisture predict soil carbon losses upon rewetting in a perennial semiarid steppe in SE Spain. Geoderma 287:2959–2975. doi:10.1016/j.geoderma.2016.06.025

Rice, A.K., J.E. McCray, and K. Singha. 2018. Methane leakage from hydrocarbon wellbores into overlying groundwater: Numerical investigation of the multiphase flow processes governing migration. Water Resour. Res. 54:2959–2975. doi:10.1002/2017WR021365

Roy, N., J. Molson, J.-M. Lemieux, D. Van Stempvoort, and A. Nowamooz. 2016. Three-dimensional numerical simulations of methane gas migration from decommissioned hydrocarbon production wells into shallow aquifers. Water Resour. Res. 52:5598–5618. doi:10.1002/2016WR018686

Scheutz, C., and P. Kjeldsen. 2004. Environmental factors influencing attenuation of methane and hydrochlorofluorocarbons in landfill cover soils. J. Environ. Qual. 33:72–79. doi:10.2134/jeq2004.7200

Selker, J.S., M. Niemet, N.G. Mcduffie, S.M. Gorelick, and J.-Y. Parlange. 2006. The local geometry of gas injection into saturated homogeneous porous media. Transp. Porous Media 68:107–127. doi:10.1007/s11242-006-0005-0

Sihota, N.J., and K.U. Mayer. 2012. Characterizing vadose zone hydrocarbon biodegradation using carbon dioxide effluxes, isotopes, and reactive transport modeling. Vadose Zone J. 11(4). doi:10.2136/vzj2011.0204

Sihota, N.J., K.U. Mayer, M.A. Toso, and J.F. Atwater. 2013. Methane emissions and contaminant degradation rates at sites affected by accidental releases of denatured fuel-grade ethanol. J. Contam. Hydrol. 151:1–15. doi:10.1016/j.jconhyd.2013.03.008

Sihota, N.J., O. Singurindy, and K.U. Mayer. 2011. CO_2-efflux measurements for evaluating source zone natural attenuation rates in a petroleum hydrocarbon contaminated aquifer. Environ. Sci. Technol. 45:482–488. doi:10.1021/es1032585

Steelman, C.M., D.R. Klazinga, A.G. Cahill, A.L. Endres, and B.L. Parker. 2017. Monitoring the evolution and migration of a methane gas plume in an unconfined sandy aquifer using time-lapse GPR and ERT. J. Contam. Hydrol. 205:12–24. doi:10.1016/j.jconhyd.2017.08.011

Strack, M., E. Kellner, and J.M. Waddington. 2006. Effect of entrapped gas on peatland surface level fluctuations. Hydrol. Processes 20:3611–3622. doi:10.1002/hyp.6518

Strack, M., and J.M. Waddington. 2008. Spatiotemporal variability in peatland subsurface methane dynamics. J. Geophys. Res. Biogeosci. 113:G02010. doi:10.1029/2007JG000472

Sudicky, E.A., and W.A. Illman. 2011. Lessons learned from a suite of CFB Borden experiments. Groundwater 49:630–648. doi:10.1111/j.1745-6584.2011.00843.x

Sudicky, E.A., W.A. Illman, I.K. Goltz, J.J. Adams, and R.G. McLaren. 2010. Heterogeneity in hydraulic conductivity and its role on the macroscale transport of a solute plume: From measurements to a practical application of stochastic flow and transport theory. Water Resour. Res. 46:W0150. doi:10.1029/2008WR007558

Tomlinson, D.W., N.R. Thomson, R.L. Johnson, and J.D. Redman. 2003. Air distribution in the Borden aquifer during in situ air sparging. J. Contam. Hydrol. 67:113–132. doi:10.1016/S0169-7722(03)00070-6

Trumbore, S. 2000. Age of soil organic matter and soil respiration: Radiocarbon constraints on belowground C dynamics. Ecol. Appl. 10:399–411. doi:10.1890/1051-0761(2000)010[0399:AOSOMA]2.0.CO;2

Watson, T.L., and S. Bachu. 2009. Evaluation of the potential for gas and CO_2 leakage along wellbores. SPE Drill. Completion 24:115–126. doi:10.2118/106817-PA

Whiticar, M.J., and E. Faber. 1986. Methane oxidation in sediment and water column environments: Isotope evidence. Org. Geochem. 10:759–768. doi:10.1016/S0146-6380(86)80013-4

Xu, L., X. Lin, J. Amen, K. Welding, and D. McDermitt. 2014. Impact of changes in barometric pressure on landfill methane emission. Global Biogeochem. Cycles 28:679–695. doi:10.1002/2013GB004571

Zhang, Y., T. Sachs, C. Li, and J. Boike. 2012. Upscaling methane fluxes from closed chambers to eddy covariance based on a permafrost biogeochemistry integrated model. Global Change Biol. 18:1428–1440. doi:10.1111/j.1365-2486.2011.02587.x